Damping Rings

Introduction and General Description

The SLC damping rings consist of separated function FODO lattices with insertions for injection and extraction. The RF cavities are also located in these insertions. The dipole magnets operate close to saturation with 2T magnetic field. Chromaticity is corrected with permanent magnet sextupoles located near the quadrupoles.[1] There are two bunches in each ring with typical populations of 4.5×10^{10} per bunch. Injection is at 120 Hz although the electron and positron damping rings have different fill cycles and store times. Many of the initial design choices are reviewed in the SLC Design Handbook,[2] and basic parameters as operated during the time period covered by this paper are given in Table DR1.

The damping rings have many features in common with third generation, low emittance synchrotron light sources. The principal differences are a small circumference and limited space along the beam line, continuous injection at 120 Hz with average injected beam powers of 1 to 2 kW, and a FODO rather than a Triple Bend Achromat lattice. The consequences of the first two are discussed in the section on operational issues.

While the electron and positron damping rings have many features in common, there are some substantive differences:

1) Injected emittances: The injected invariant emittances are roughly $\gamma\varepsilon_x \sim \gamma\varepsilon_y \sim 2\times10^{-4}$ m for electrons and roughly $\gamma\varepsilon_x \sim \gamma\varepsilon_y \sim 1\times10^{-3}$ m for positrons.
2) Fill Pattern and Store Time: Two electron bunches spaced forty 714 MHz wavelengths apart are injected on the same SLC cycle, damp for 8.3 msec, and are extracted on the next SLC cycle. The first of these bunches is the "production" bunch that collides with positrons at the interaction point. The second is the "scavenger" bunch that is targeted onto a converter to produce positrons for subsequent cycles. One positron bunch is injected on each SLC cycle. It is positioned diametrically opposite to the bunch that remains from the previous cycle (forty-two 714 MHz wavelengths). This injected bunch is stored, damps for 16.6 msec, and is extracted two cycles later. These different fill patterns affect injection and extraction kicker requirements and transient beam loading.
3) Magnetic Circumference: The magnetic circumference of the electron damping ring was increased by 9 mm over the nominal orbit circumference of 35.27 m to increase the horizontal damping partition number to $J_x = 1.15$ and thereby reduce the horizontal damping time and equilibrium emittance. The magnetic and orbit circumferences of the positron damping ring are equal because the acceptance needs to be larger for the larger injected emittances.

The damping rings were designed for operation at 1.21 GeV. The electron beam is longitudinally polarized at the point where it leaves the linac and enters the linac-to-ring transfer line (LTR). The design was to have the spin precess from longitudinal to horizontal polarization in the 163.9° bend before reaching a 6.32 T-m solenoid that rotated it vertically to preserve polarization during damping. A small sacrifice of less than 1% in polarization was taken by operating at 1.19 GeV. This was done to improve

Table DR1: SLC Damping Ring Parameters[3,4]

Energy	1.19 GeV
Typical Population per Bunch	4.5×10^{10}
Orbit Circumference	35.27 m
Revolution Frequency	8.5 MHz
Bending radius	2.037 m
Bending Field	1.948 T
Approximate Injected Emittance (e^+, e^-)	1×10^{-3}, 1×10^{-4} m
Approximate Injected Energy Spread (e^+, e^-)	XXX
Approximate Tunes (Horizontal, Vertical)	8.23, 3.43
Approximate Quadrupole Gradients (F, D)	6.2, 7.3 kG/cm
Momentum Compaction	0.015
RF Frequency	714.000 MHz
Harmonic Number	84
Typical RF Voltage	V_{RF} = 800 kV
RF Cavity Properties	
Load Shunt Impedance	2.5 MΩ
Loaded Quality Factor	6860
Coupling	2.5
Typical Synchrotron Tune	Q_S = 0.012
Radiation Integrals (Soft Edge Model)[4]	
I_2	2.805 m^{-1}
I_3	1.3595 m^{-2}
I_4 (for J_x = 1.01, 1.15)	-0.027, -0.421 m^{-1}
I_5	0.01748 m^{-1}
Energy Loss/turn from Synch Radiation	79.2 keV
Energy Damping Time (J_x = 1.01, 1.15)	1.78, 1.91 msec
Horizontal Damping Time (J_x = 1.01, 1.15)	3.50, 3.07 msec
Vertical Damping Time	3.53 msec
Fractional Equilibrium Energy Spread (J_x = 1.01, 1.15)	7.12×10^{-4}, 7.39×10^{-4}
Zero Current Bunch Length (Q_S = 0.012; J_x = 1.01, 1.15)	16.7, 17.3 psec
Horizontal Emittance (Zero Coupling, J_x = 1.01, 1.15)	$\gamma\varepsilon_x = 2.99\times10^{-5}$, 2.63×10^{-5} m
Approximate Vertical Emittance (10% coupling)	$\gamma\varepsilon_y \approx 3.0\times10^{-6}$ m

Notes

The electron (positron) damping ring is located north (south) of the linac and is often called the North Damping Ring (South Damping Ring).

The quoted emittances are invariant emittances.

The radiation integrals and quantities derived from them are theoretical values.

reliability and to reduce saturation in the dipoles so that trim windings would have enough range for steering.

Many of the components of the SLC damping rings are standard in terms of design, specification, and performance. In the following section we deal with those components that were special in some way, and then we turn to operational and beam dynamics issues.

Damping Ring Components

Vacuum Chamber: Prior to 1993 there was a longitudinal, single-bunch instability that limited the SLC beam to 3×10^{10} particles per bunch. [5] It would manifest itself as periodic variation in the bunch phase with respect to the ring RF. The phase was responding to changes in the bunch length through the bunch length dependence of the higher order mode losses. The bunch length would blow-up rapidly whenever the peak current exceeded a threshold. This blow-up followed by relaxation due to radiation damping could be observed directly on a peak current detector, where it was dubbed as the "saw-tooth" instability. If the bunch length blow-up and corresponding jump in beam phase happened to coincide with extraction, an errant pulse or "flyer" would be observed in the linac with the wrong energy and bunch parameters. It was possible to influence the onset of the instability by increasing the bunch length during the store time by ramping down the RF voltage, as described in the section on the RF system.

However, increasing the intensity significantly required a new vacuum chamber with reduced inductance, the dominant contribution to the impedance at the operating bunch length. This chamber was installed prior to the 1994 – 1995 SLC run. Table DR2 compares the inductances of the new and old vacuum chambers.

Table DR2: Vacuum Chamber Inductance[6]

Element	Old Chamber[7] (nH) †	New Chamber[8] (nH)
Synchrotron Radiation Masks	9.5	----
Bellows	----	1.1
Quadrupole-to-Dipole Chamber Transitions	9.3	2.4
Ion Pump Slots	0.2	0.05
Kick Magnet Bellows	4.1	----
Flex Joints	3.6	----
Beam Position Monitors	3.5	0.2
Other	2.4	2.4
Total	**33**	**6**

† The bellows included in Table 1 of reference 7 were shielded in a previous upgrade. Changes to that table from recent calculations are included here.

The synchrotron radiation masks and flex joints in the old chamber were associated with chamber flexibility. The masks protected bellows at one end of each four-foot long chamber section, and the flex joints added flexibility to the middle of each section. Flexibility was needed to compensate for limited precision in the adjustment of magnet positions and variations in chamber geometry in fabrication. Part of the design of

the new chamber was magnet and vacuum chamber mounts capable of being surveyed and positioned to ±100 μm. In addition, the chambers were assembled in eight foot sections in a precision fixture that positioned parts prior to welding and provided a jig for minor adjustments after welding. By using these techniques flex joints became unnecessary and the numbers of bellows could be reduced by a factor of two. Synchrotron radiation masking was incorporated into the bellows RF shield, so the net change in the inductance from bellows and flex joints was from 13.1 nH to 1.1 nH.

The vacuum chamber profile is rectangular in the dipoles to minimize the gap and thereby increase the magnetic field and reduce the damping times, and the profile is circular in the quadrupoles to provide adequate aperture. Modern materials and machining techniques allowed the quadrupole-to-dipole chamber transitions to be made smoothly over 5 cm versus 6 mm in the old chamber. Dispersion strengthened copper, Glidcop*, was chosen for the combination of strength and thermal conductivity needed to conduct away heat from synchrotron radiation. The transition was made smooth by electrodischarge machining a continuous change from a circular to a rectangular profile over the length of the transition.

Other changes were the redesign of the beam position monitors and the slots between the beam and distributed ion pump chambers. The beam position monitors were made at the same radius as the beam pipe itself instead of being recessed. The pump slots were made narrower and deeper to cut-off high frequency fields, and several slots were used instead of one to maintain pumping speed. Finally, the bellows at the ends of the ceramic beam pipes for the injection and extraction kicker magnets were shielded.

The real part of the impedance has been measured by measuring the shift of the synchronous phase with current. The loss factor at V_{RF} = 760 kV where the zero current bunch length is 5.4 mm was measured to be 16.0 ± 2.4 V/pC, corresponding to a resistance of 1 kΩ.[9] This is in good agreement with the calculated value of 15 V/pC.[8]

The consequences of the vacuum chamber impedance reduction were unexpected. The instability threshold was lowered from 3.0×10^{10} to $1.5 - 2\times10^{10}$ particles per bunch. Rather than increasing the threshold, the limiting amplitude of the instability was reduced such that it no longer limited the SLC current although beam jitter associated with the damping ring instability was observable in the linac.[10] The phenomenology of the instability is treated in the beam dynamics section.

Injection and Extraction Kicker Magnets: The damping rings require injection and extraction kicker magnets that *a)* give a 7 mrad kick, *b)* have rise and fall times of less than 60 nsec including thyratron pulser rise and fall times, *c)* fit into the available space of less than 50 cm along the beam line, and *d)* work in localized radiation levels of roughly 10^7 to 10^8 rads/hour, estimated from dosimetery measurements made near the beam pipe. The kickers in the electron damping ring must inject and extract two bunches on a single pulse. This requires a pulse with a 60 nsec long flattop and the kicks to the two bunches differing by less than 10^{-3}.

The third generation of kicker, a matched, terminated transmission line C-type magnet constructed with radiation hard, alumina-loaded epoxy met all of these requirements.[11] Each kicker is a segmented LC circuit with the flux return provided by a

---

* Glidcop is a product of OMG Americas, Research Park Triangle, NC.

short path of high permeability ferrite and capacitance obtained from radial plates. Placing the central conductor to one side of the beam pipe reduces stray inductance. This forces all the flux to enter the beam pipe. Each magnet has 8 LC cells; it is shown in cross section in Figure DR1. The high voltage (HV) and ground plates form the capacitor. The dielectric is 1 cm thick Conapoxy FR-1727 epoxy[†] that is 50% aluminum oxide powder by weight. There is a 30° wedge removed from the magnet to allow it to be installed over the beam pipe. The wedge contains a ground electrode that forces stray magnetic field through the beam pipe.

The beam pipes are ceramic tubes with a thin metallic coating inside to shield the high frequency wall currents associated with the beam. Ceramic gaps at each end isolate the coating from ground to avoid a shorted turn. The region between the beam pipe and the magnet is filled with XXX dielectric grease[§] to prevent voids that could lead to arcing. Magnet and beam pipes are assembled into integral units that are tested under vacuum and installed without removing the beam pipe from the magnet.

The performance of the magnets themselves has been excellent. They behave like matched transmission lines with negligible ringing or other imperfection. The transit time is less than 35 nsec. The major problem has been beam pipe failures caused by arcing and corona. These failures were often catastrophic with the beam pipe fracturing and venting the vacuum system to atmosphere. In one case protection interlocks failed to shut off the high voltage pulser, and the kicker caught fire and contaminated a substantial length of the electron damping ring chamber with hygroscopic combustion products. Recovery from this and subsequent ventings was extremely slow.

The beam pipe evolved from having a ceramic gap at one end with the other end grounded to the present design in response to failures.[11] The initial design failed due to pin hole leaks at the ceramic gap caused by corona and due to arcs at the grounded end. Encapsulating the gap in epoxy cured the corona, but that change was short-lived. In one instance the epoxy melted due to higher order mode power and in another it caught fire when the chamber arced at the grounded end. Several beam pipes failed due to arcs at the grounded end that caused the pipes to fracture. This was fixed on a temporary basis by disconnecting the ground by abrading away a short length of the coating. The permanent cure was to have ceramic gaps, designed to withstand the voltage without epoxy, at each end. A bellows shield near the ceramic gap was also redesigned to avoid arcing inside the chamber to the spring fingers of the shield. Such arcing appears to have caused one beam pipe fracture.

One additional failure mode has been encountered since those documented in reference 11. Radiation damage from injected beam loss caused the kicker epoxy to swell and to partially extrude the wedge. This led to an air gap between the magnet and beam tube and arcing from high voltage to the chamber coating. Careful alignment minimized injected beam loss on the kicker itself and reduced the failure rate significantly. There were no failures during the XXX months between the time the kickers were aligned and the 1997 – 1998 run ended.

[†] Manufactured by CONAP, Olean, NY

[§] XXX reference to type and manufacturer of dielectric grease

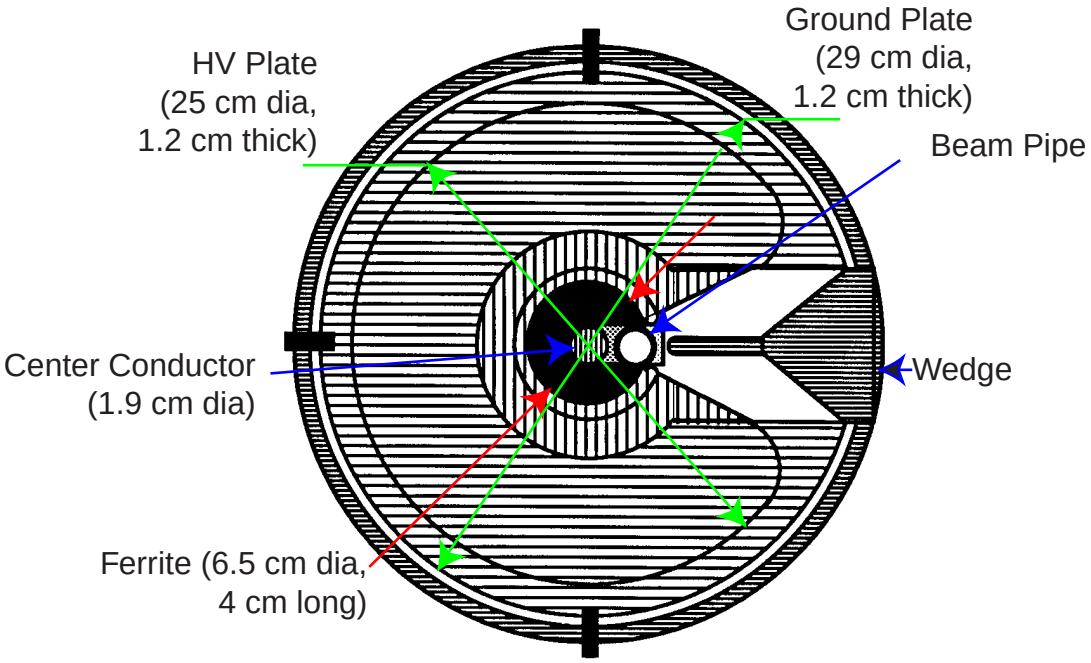

Figure DR1: Cross section view of the kicker magnet.[11] The high voltage plate is vertically hatched and is largely hidden behind the horizontally hatched ground plate. The longitudinal dimensions are per LC cell. Details of the construction are contained in reference 11.

Septum: [12] Two DC septum magnets connected in series are used for injection and another two septa, identical except for a 180° rotation, for extraction. The extraction septa are wired in series with a dipole magnet that is 180º away in phase to relieve the tolerances on the power supply that must be regulated to XXX. The first injection septum is 12 mm thick, and the magnetic field and bend angle are 0.77 T and 8.34º, respectively. The second magnet, which is close to the stored beam orbit, has a thin, tapered septum that is 39.4 cm long and 3 mm thick on one end and 8.8 mm thick on the other. The maximum current density is 120 A/mm^2. The magnetic field is 0.3 T, and the bend angle is 1.76º. The thin septum carries 2600 A and is cooled with two 3/32" outside diameter, 0.015" wall thickness stainless steel tubes.

There is a copper liner along the stored beam orbit to minimize the impedance presented to the beam, and backleg windings are provided to minimize stray magnetic field for the stored beam. Localized ion trapping was a concern so the vacuum jackets were pumped with XXX (pumping speed and number) ion pumps. The magnets were supported on ceramic stand-offs and their positions transferred to tooling balls on the outside of the vacuum jacket for septum alignment. Alignment was difficult because the septum jacket had to mate to a transfer line and to the damping ring in two places. In addition, over time the ceramic stand-offs cracked and had to be replaced so the septa could be aligned.

The magnetic field in the extraction channel was measured and found to have position dependent components

$$\Delta x' = 46\ \mu r \cdot e^{-kx} \cos(ky)$$
$$\Delta y' = -46\ \mu r \cdot e^{-kx} \sin(ky)$$

where x is the horizontal distance from the current sheet, y is the vertical coordinate with y = 0 in the center of the channel, and k ~ 1.16 mm^{-1}. These led to highly position dependent, local, normal and skew quadrupole fields that had the potential of blowing-up the extracted beam emittance through mismatch from the normal quadrupole in the horizontal and coupling due to the skew quadrupole in the vertical. These effects could be minimized by centering the beam vertically and kicking the beam at least 2.5 mm inside the channel. These requirements could be met but required continual maintenance of the orbits in the septum region.

RF System: For each SLC damping ring, the RF system has a single klystron powering two 2-celled copper accelerating cavities installed roughly opposite each other.[13] The cavities were designed to achieve a peak accelerating potential in excess of 1 MV. Each cavity includes a ceramic window in the input waveguide, a slot coupling from the waveguide into one of the structures' 2 cells, and 1 fixed and 1 moveable tuner. The two cavities are driven by a single klystron through an isolator and a waveguide magic tee to prevent reflected power from the cavities reaching the klystron. The cavities are pumped with twin 80 l/sec pumps in the electron damping ring and XXX pumps in the positron damping ring. Beam and cavity parameters are given in Table DR1.

The low-level RF system has evolved to keep up with the demands of higher beam current. The basic configuration consists of a Voltage Control Oscillator, locked to a harmonic of the linac Main Drive Line, providing power to the klystron via several attenuators and phase shifters that are the actuators for the RF feedback loops. A servo-controlled mechanical tuner in one cell of each cavity maintains a constant loading angle. This loop responds to changes in temperature, beam current or beam rate with a time constant of several seconds. A gating system has been incorporated to improve the response of the system during rate changes imposed by the downstream Machine Protection System.

The phase compensation loop maintains a constant phase between the klystron and cavity. This loop allows adjustment of the cavity tuning angles without having to make a compensating change in the injection phase of the beam that has a tolerance of only a few degrees at high currents. The phase shift across the klystron depends on its supply voltage, and the phase compensation loop is also able to compensate for power supply variations. The bandwidth is high enough to reduce phase noise on the beam caused by 360 Hz power supply ripple.

The amplitude feedback regulated the sum of the magnitudes of the RF voltages in the two cavities with a bandwidth of several kHz. The sum of magnitudes is proportional to the total RF voltage when the two cavities have the same tune, but it was not always possible to operate in that way. That led to RF settings that were not reproducible from day-to-day. The feedback needs to be redesigned to regulate the magnitude of the vector sum of the cavity voltages.

The "S-band phase loop" locks the phase of the damping ring beam, determined from a filtered stripline pick-up signal, to the S-band phase of the bunch compressor and main linac. The gain-bandwidth is sufficient to reduce the phase noise of the extracted bunch to below 0.5° S-band. This loop is gated. It switches on 1.3 msec after injection and then ramps to the extraction phase. Effectively, it decouples the injection and

extraction phases and makes the extraction phase independent of any phase drifts in the injector. In addition, the electron and positron S-band loops allow independent control of the beam phases at injection into the main linac.

A vector, or direct RF feedback[14] is a high bandwidth loop immediately around the klystron and cavities. It was initially installed to raise the Robinson high current limit[15] that was encountered when the RF voltage was lowered to control the bunch length.[16] Although this limit was not as important in the later phases of SLC operation, the direct feedback loop was routinely used to minimize transient beam loading at injection and extraction and to reduce RF noise.

Π-Mode Cavity: A longitudinal, coupled bunch, π-mode instability was observed in early SLC operations. The threshold was approximately 1×10^{10} particles per bunch, and it depended on the RF cavity temperatures and tuning angles. This instability is damped with a passive cavity installed in 1992.[17] The resonant frequency is 1062.4 MHz which is just below the 125th harmonic of the rotation frequency. This harmonic was chosen so that a single cavity design could be used for both rings. It is near a maximum of the π-mode spectrum in the electron damping ring where the bunches are not equally spaced and yet is an odd harmonic as required for the positron damping ring with equally spaced bunches. Each cavity has a single cell and has one fixed and one movable tuner to allow the flexibility needed to damp the longitudinal instability without exciting a transverse coupled bunch instability. The shunt impedance and quality factors are 1.8 MΩ and 15,000, respectively. These give a damping time of approximately 100 μs for two bunches of 5×10^{10} particles/bunch. This is one-tenth the measured growth time.

Diagnostics: The diagnostics in the transfer lines to and from the damping rings, included toroids, beam position monitors, fluorescent screens, and wire scanners. Toroids were used primarily to determine the current transmission through the beam lines and the damping ring. These toroids are calibrated to XXX% absolute, but there can be systematic errors of XXX% or more in regions of high particle losses. This was the case in the positron injection line where the injected beam had large emittance and energy spread and suffered roughly XXX% loss in the line. The screen in the early part of the extraction line was used primarily as a diagnostic of the beam proximity to the bad-field region of the extraction septum. Single wires were located at a high dispersion region of the injection line for monitoring the incoming energy spread, and in the extraction line to monitor beam sizes, and, occasionally, to measure the beam emittance using quadrupole scans or the energy spread by making modifications to the local lattice. The first multiple-wire emittance monitor was located in the linac just upstream of the first accelerating structures.

In the damping ring proper, diagnostics included beam position monitors (BPM's), synchrotron light monitors, and analogue devices for the RF system. The BPM's were 3.2 cm long, 2.45 cm inner diameter, XXX Ω striplines located at each quadrupole. The position of a particular bunch on a particular turn could be measured to give the injection, stored, and extraction orbits for each of the two bunches. The readout was multiplexed with one-sixth of the BPM's read out during one damping ring cycle. The single measurement resolution was approximately XXX μm. While this could be improved with averaging for many purposes that was not always appropriate. In particular, improved BPM resolution would have been useful to track jitter observed in

the linac back into the damping rings to locate the source, but the jitter was below the BPM resolution, so this was not possible.

A few BPM's were reserved for special uses including turn-by-turn betatron tune measurements,[18] measurement of the beam phase for locking the beam to the RF phase in the downstream linear accelerator,[19] and instability diagnostics.

The visible synchrotron light produced in an arc bending magnet is extracted from the vacuum chamber with a precision-aligned, water-cooled molybdenum mirror and focused with a steerable, off-axis parabolic mirror.* The light is transported approximately 20 m to an auxiliary building on the surface that allows easy access for standard and specialized cameras and associated hardware. The two specialized cameras that were used for many measurements were a fast-gated camera and a streak camera. The fast-gated camera, Xybion ISG-250, allowed imaging of a single bunch on a single revolution.[20] The readout was a standard TV scan, so only one image could be acquired per damping ring store. The streak camera was a Hamamatsu FESCA 500 with an 0.5 psec resolution. It could run in a stand-alone mode or in a mode where the image acquisition was controlled by the accelerator control system to allow correlation with other SLC variables. In either mode the image acquisition rate was 0.1 Hz or less.

Operational Issues

Injector Power and Beam Loss: A significant difference between third generation light sources and damping rings is the high average power of the injected beam. The injection rate for the SLC damping rings was 120 Hz, and the average injected beam powers were roughly 2 kW and 1.2 kW for the electron and positron rings, respectively. The electron damping ring capture efficiency was 90% - 95% during routine operation, so there was 100 - 200 W of beam loss in the ring. The positron ring capture efficiency was lower, 70% to 80%, because of the larger incoming emittance, so the beam loss was roughly 200 W there also.

The cumulative radiation damage associated with this beam loss had important operational consequences. It was a major cause of kicker magnet failures, and the permanent magnet sextupoles were replaced in 1994 because of radiation damage to epoxy. Dipole and quadrupole coils were radiation damaged and had to be replaced. All of the dipole coils in the electron damping ring have been replaced with a design that is less susceptible to corrosion damage of the coil braze joints, and the dipoles in the positron damping ring are scheduled for a similar retrofit. Most of the quadrupole coils have been replaced because of corrosion associated with the incorrect use of teflon as a jointing compound. Teflon breaks down under radiation into aggressive chlorinated compounds.

An arc in a radiation damaged vac-ion pump cable caused a fire that did extensive damage to the control and power-distribution cable plants of electron damping ring and

---

* Originally the light was steered by a moveable mirror in the vacuum and achromatic transmission optics were used. The moveable mirror was replaced with the fixed mirror because higher-order mode heating of the mirror bellows resulted in several catastrophic vacuum vents, and the transmission optics was replaced with reflective optics because of radiation damage.

spewed corrosive combustion by-products throughout the damping ring vault. More than a month of running time was lost recovering from this fire.

RF System: The typical damping ring beam during the 1997 - 1998 run was 4 - 4.5×10^{10} particles per bunch corresponding to peak and average currents of approximately 120 A and 120 mA, respectively. These large currents caused a number of operational issues for the RF system.

First, the Machine Protection System, described in section XXX, limited the repetition rate when certain faults were detected in systems downstream of the damping rings. This led to damping ring cycles without any beam, and these had to be accommodated. Because of heavy beam loading a cavity tuned with beam present would be grossly mismatched without beam. One possible consequence is that the cavity tuner feedback loops would start to tune the cavity thereby leading to another mismatch when full repetition rate was restored. This was avoided by inhibiting cavity tuning during pulses without beam. Another possible consequence was that the klystron could be driven into saturation because, nonintuitively, the mismatched cavity without beam requires more power than the matched cavity with beam.[21] Regulation loops would lose gain, and in some cases could even switch from having negative to having positive feedback.[21] This was solved in part with an intermediate, reduced voltage reference level for the amplitude feedback loop when there was no beam and by operating with a positive loading angle.

The RF cavities were and still are plagued by vacuum activity that at times led to RF window leaks.* Our experience was that the cavities could not be operated reliably above 1×10^{-7} T without risking a window failure. This was set as the trip level to inhibit the RF. Ambient operating pressures were an order of magnitude lower, but often vacuum bursts exceeded the trip level. One cause was heating of the ion pumps by beam induced RF. Placing RF shields over the pump openings solved this problem. Another cause of trips was multipacting in the tuners caused by beam induced higher modes. This was evidenced by particular tuner positions with increased vacuum activity with beam present, and it remains to be fixed with a new tuner design. We operated by tuning the two cavities such that there was no multipacting in either one. However, this did not always work and could led to frustrations particularly when repetition rate changes caused thermal changes to the cavity. In addition, because the amplitude controller assumed that the cavities had the same tune, and RF settings were not reproducible from day-to-day.

Bunch precompression was sometimes used to increase the linac current. Transverse aperture restrictions in the ring-to-linac transport line (RTL) are important at high current. The RTL contains a bunch compressor that introduces a large energy variation across the bunch and hence a large transverse beam size due to dispersion. The compressor amplitude was increased in 1994 to shape the bunch distribution (see section XXX); this increased the energy spread and beam loss. Moreover, due to bunch

---

* Replacing a window could take several weeks. The first failed window was replaced, and the leak traced to a pinhole. As an experiment the second failure was sealed in place by spraying the window itself with a light coating of VacSeal, manufactured by Space Environment Laboratories, Boulder, CO. This was effective as a temporary fix, and it became the routine repair technique.

lengthening in the damping ring, the higher the beam current, the higher the loss. To avoid such losses, the bunch length was precompressed in the damping ring with two, appropriately timed, rapid changes in RF voltage that introduce a longitudinal mismatch with an elongated bunch. This was shown to work, but to be unstable. [22]

The instability was traced to the RF feedback loops driving the klystron into saturation and losing regulation. With this understanding we installed a remotely adjustable, non-linear limiter into the klystron drive circuit, and changes in the klystron gain were compensated whenever the klystron was replaced. However, the maximum power levels of the klystrons varied by approximately 20%, and it was difficult to compensate for a klystron with low maximum power without raising the high voltage, which reduced the tube lifetime. With the limiter installed bunch precompression was successfully used in the electron damping ring to increase the product of the electron and positron currents at the interaction point by 15 to 20%. Part of that increase was due to increased current at the positron production target. It was not possible to routinely use bunch precompression in the positron ring because of unrelated problems with the cavity tuners.

Modeling: Quadrupole and corrector magnetic field values were measured directly, and, independently, they could be determined from beam-based measurements. There were significant discrepancies between the results of these two measurement techniques. The differences for the correctors ranged from 10% to 40% depending on whether they were vertical or horizontal and were in the electron or positron damping ring. The effective quadrupole gradients were between 0.9% and 6.5% lower than the directly measured values for the different quadrupole families and rings. These differences varied from year to year.

These field errors resulted from design decisions to maximize radiation damping: small ring circumference, high packing factor, and dipoles well into saturation with B ~ 2 T. The correctors were trim windings rather than separate magnets. The horizontal correctors were trims on the saturated dipoles, and the vertical correctors were trims on the quadrupoles. Initially chromaticity was to be corrected by shims at the end of the dipoles. This did not work because of saturation, and permanent magnet sextupoles had to be installed in limited available space with no possibility of alignment.[1] A comprehensive study of fitting beam orbits when each of the ring correctors was perturbed has shown that the quadrupole gradient errors can be completely accounted for by orbit offsets in the sextupoles. One other consequence of the tight packing was that the fringe fields could not be modeled properly due to the interaction between closely spaced, neighboring magnets.

Accurate knowledge of the field strengths was necessary for control of the emittance and orbit. As examples, orbit correction was based on singular value decomposition which requires a model of the optics,[23] and closed bumps in the injection and extraction region were needed for routine tuning of injection efficiency and equilibrium emittance. In practice the relative field errors were measured and incorporated as ‘fudge factors’ into the online model.[24] The corrector errors were obtained by beam-based measurement of the transfer matrices while the quadrupole errors were inferred from the ratio of predicted to measured betatron tunes. The corrected model was then used for subsequent orbit steering.

Injection Steering and Matching: Injection orbit errors or phase space mismatches filament and result in increased effective beam emittance that must subsequently be radiation damped. With the electron storage time only about 2.5 times the nominal transverse damping time, injection errors were a potentially serious source of emittance growth.

Figure DR4 shows the synchrotron light images for the first twelve turns after injection into the electron damping ring when it was fully coupled with fractional tunes near the quarter integer.[20] The distribution varied dramatically from turn-to-turn. This can be explained in part by the injection septum field that cannot be parameterized as only a quadrupole given the injected beam size. After about 10 μsec when the beam had filamented the images were elliptical as expected for Gaussian distributions.

Injection was improved by first minimizing the difference between the first turn and stored beam orbits using beam position monitors and then by properly orienting the phase space using several quadrupoles at the end of the injection line to minimize the filamented beam size at turn 1250.

The degree of mismatch was characterized by taking the Fourier transform of the rms beam sizes obtained with the gated camera.[25] Typically 100 turns of data were acquired. Examples are shown in Figure DR5. The peaks at the betatron frequency and at its second harmonic indicate the presence and size of dispersion and betatron mismatches, respectively.

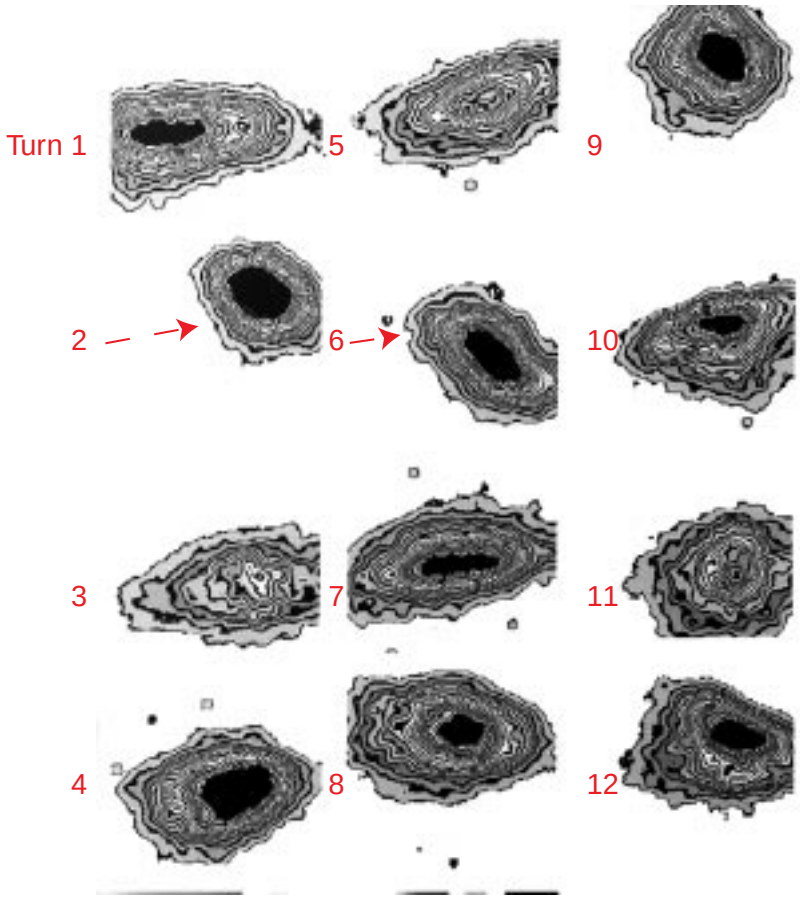

Figure DR4: Beam images for the first twelve turns in the electron damping ring with $Q_x \approx Q_y \approx 0.25$. Successive turns correspond to different beam pulses. It was verified that the distribution was reproducible from pulse-to-pulse.

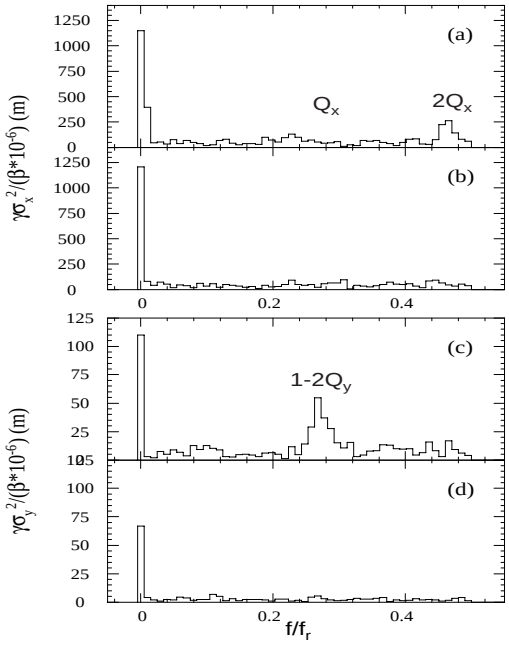

Figure DR5: Fourier transforms of the measured rms beam sizes before (a) & (c) and after (b) & (d) injection matching in the electron damping ring in the horizontal and vertical planes, respectively.

Thermal Effects: The thermal effects that have been observed fall into two basic categories. There are long time constant drifts of several days associated with the gradual heating of the concrete vault and ring support structures from the power dissipated by the dc magnets, on top of which there is also a slower seasonal variation. Short time constant variations are also observed with the turning on and off of the beam, where the synchrotron radiation heating of the vacuum chamber causes expansion and contraction over a period of minutes.

The damping rings are located approximately 30 ft underground in concrete vaults with wall thickness up to 4½ ft and consequently have a large thermal inertia. The dc magnets have a combined power dissipation in excess of 1 MW per ring that must be removed by the water-cooling. The unusually high packing fraction of the ring gives the damping ring the highest power density of all the accelerator housings on the SLAC site. The temperature of the return circuit of the cooling water is fairly high, and a significant fraction of the heat is also dissipated in the air resulting in an equilibrium air temperature close to 105^o F. In order to avoid diurnal and seasonal temperature variations the access shafts to the vaults have been sealed and there are also airtight radiation doors isolating the rings from linac tunnel. Before any access to the rings can be made for repair or maintenance the vault air must be purged, resulting in a large temperature swing. During beam tuning after a ring access we observed closed orbit errors of several mm which we attribute to the expansion of the concrete support girders for the ring magnets. The concrete support girders are divided into quadrants plus two "Y" girders at the injection

and extraction regions. These curved concrete sections are supported on steel jacks and can bow considerably with changes in temperature. After a 20^o F cool down thermal equilibrium would only be reached again after 1 week, so we have installed large space heaters in the vaults which shorten this recovery process to 24 hours.

The thermal properties pose a problem for initial alignment of the ring components by the survey crews since they cannot work under the conditions of the normal operating temperature. Instead, they make an empirical estimate of how much the ring circumference will expand and do a compensated alignment when the vault temperature is 85^o F.

The slow thermal drifts cause problems with ring circumference, but the short-term thermal effects associated with the beam presence manifest themselves in the extracted orbit. The synchrotron radiation power is dissipated in the water-cooled vacuum chamber, and the temperature fluctuations of the chamber appear to have an effect on its alignment, as seen by the beam position monitors. This is most noticeable around the "Y" girder of the extraction region where the orbit monitoring feedback is seen to make compensating changes for several minutes after each period of prolonged beam absence. We have tried to address this problem by putting temperature regulation on the cooling water for the vacuum chamber and heating it when the beam is absent to compensate. However, the problem is more complex and undoubtedly related to the passage of the beam through the good field region of the extraction septum, mentioned earlier, and the effect is still seen. There may be higher order mode beam heating in the septum itself, which may contribute to the problem.

Beam Dynamics

Damping Times: The damping times were measured in 1991 by changing the store time and measuring the beam size with wire scanners downstream of the electron damping ring.[26] They were longer than calculated and worrisome because of the ratio of store time to damping time. While these particular measurements were prone to systematic errors associated with the extraction line aperture, they motivated a series of damping time measurements using synchrotron light and the fast-gated camera. In a typical measurement about 50 images were obtained by advancing the camera trigger through the 8.33 msec store. Reference 20 contains details of the data analysis and systematic error checks. The data were fit to determine the injected beam size, σ_i, the equilibrium beam size, σ_e, and the damping time, τ. For example, in the horizontal

$$\sigma_x^2 = \sigma_{i,x}^2 \exp\left(-\frac{2t}{\tau_x}\right) + \sigma_{e,x}^2\left[1-\exp\left(-\frac{2t}{\tau_x}\right)\right] \quad .$$

Figure DR2 shows results obtained in 1992 after increasing the ring circumference by 9 mm to increase J_x to 1.15. The measured damping times are roughly 0.4 msec longer than expected from the soft edge model of the magnetic fields.[4]

Subsequent measurements made over many months showed that the damping changed with time.[27] The average damping times were $\tau_x = 3.32 \pm 0.28$ msec and $\tau_y = 4.11 \pm 0.14$ msec where the errors are the standard deviations of twelve separate measurements spanning two months. These variations might result in part from circumference changes which were common following ring accesses, but they are larger than can be explained by this.

In summary, the damping times are longer than calculated and have an unexplained time variation.

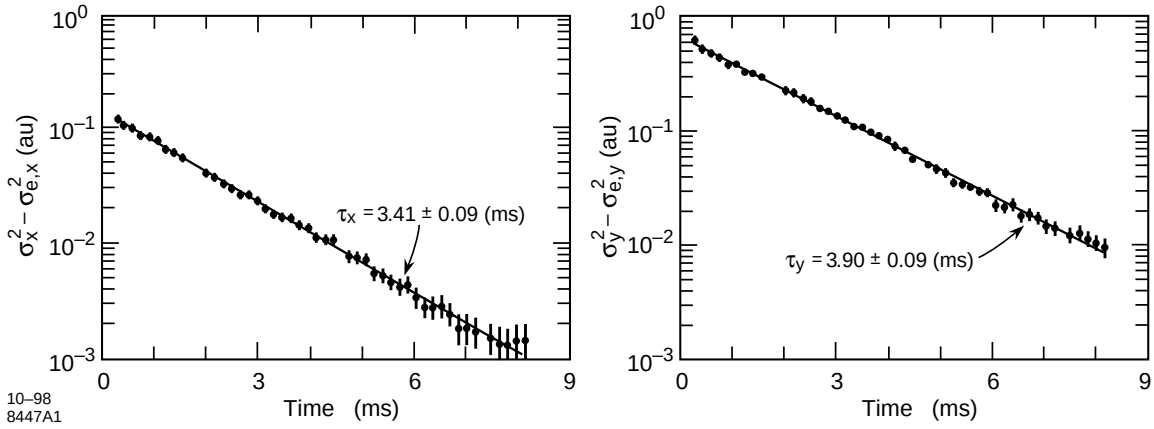

Figure DR2: Measured horizontal (a) and vertical (b) damping times in the electron damping ring. The experimental results are to be compared with the expected values of τ_x = 3.07 msec and τ_y = 3.53 msec.

Single Bunch Longitudinal Instability: With the new vacuum chamber described earlier there is a longitudinal single bunch instability with a threshold in the range $1.5 - 2\times10^{10}$ particles per bunch. The instability is seen in signals derived from a beam position monitor, Figure DR3, and by an increase in energy spread, Figure DR9. It occurs with both one or two bunches in the ring suggesting a single bunch phenomenon, and the instability properties of the electron and positron damping rings are similar. The behavior at different intensities, illustrated in figure DR3, is complex:

1) At currents below $\sim4\times10^{10}$ per bunch the instability is a quadrupole instability identified by the characteristic sidebands of the rotation harmonics at twice the synchrotron frequency. The rise time is roughly 1 msec, and at some currents the amplitude saturates while at others it behaves as a relaxation oscillation.
2) Above 4×10^{10} per bunch the instability becomes a sextupole instability. The beam position monitors are less sensitive to this mode, so the amplitude appears smaller in Figure DR3.

The SLC operated in the region 3.5×10^{10}/bunch to 4.5×10^{10}/bunch where there were strong quadrupole or sextupole instabilities. The remainder of this section deals with measurements of the instability and its consequences for the SLC.

Beam position monitor signals measure phase space structure and relative amplitudes of the instability, but, since the high frequency impedance is unknown, they do not give information about the amount of charge involved. This has been measured with the streak camera by correlating the beam position monitor signal with streak camera images.[28] The results are shown in Figure DR6. The potential well distortion of the average bunch shape and the quadrupole instability structure are clear. About 3% of the charge is redistributed by the instability.

There was jitter in the linac beam trajectories (see section XXX) that has many causes. The damping ring instability was one of them. The linac orbit was correlated with the instability signal sampled just before extraction to measure this. Figure DR7 shows that there was a clear dependence of the orbit and the linac bunch length, measured

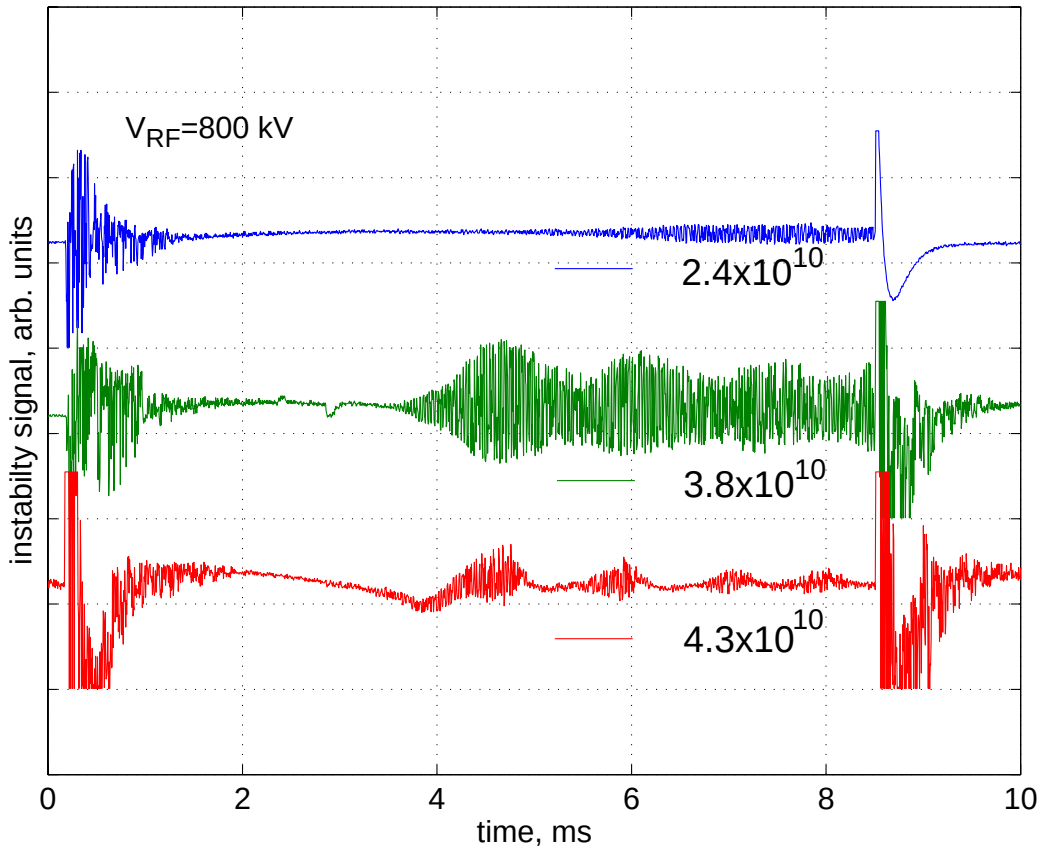

Figure DR3: Beam instability signal for different bunch intensities and an RF voltage of 800 kV. The transients at t ~ 0.3 msec and 8.6 msec are due to injection and extraction, and the signal associated with the instability is between those times. The signal is a high frequency signal, f > 6 GHz, derived from a beam position monitor.[28]

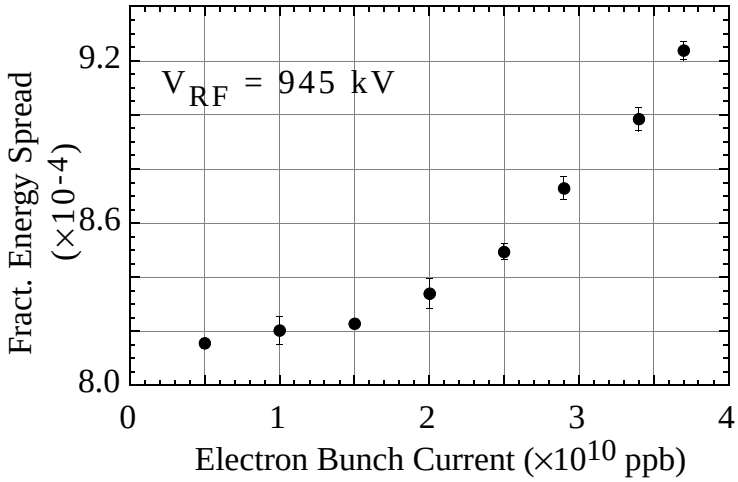

Figure DR9: Energy spread measured in the extraction line for an RF voltage of 945 kV. (Ref. 6)

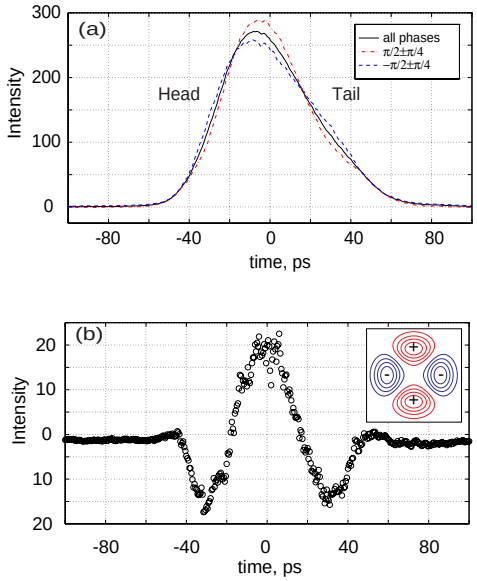

Figure DR6: The quadrupole instability at the maximum amplitude for with 3.8×10^{10} particles per bunch. (a) Beam profiles averaged over all instability phases and at $+\pi/2$ and $-\pi/2$ where the bunch is shortest and longest, respectively. (b) The instability structure determined by subtracting the average at different values of the phase.[28]

with a 36 GHz cavity pick-up,[29] on the instability. It is estimated that roughly 40% of the linac jitter power was due to the instability making it a significant, but not the only, source of jitter.[10]

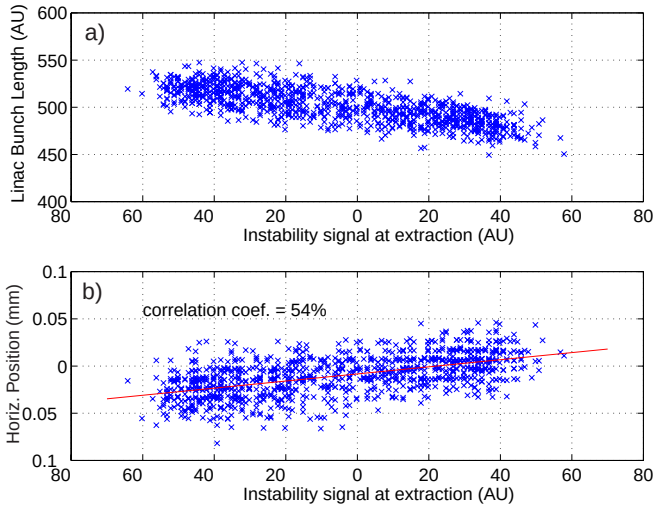

Figure DR7: Correlations of (a) the linac bunch length and (b) the horizontal beam position at quadrupole 201 in linac sector 20 with the damping ring instability signal sampled just before extraction. These data were taken with 4.1×10^{10} particles per bunch and V_{RF} = 700 kV.

Ion Effects: There was a catastrophic kicker chamber failure in the electron damping ring in 1996, and the vacuum system was contaminated for several months. During this time the vertical emittance of the extracted beam was increased by a factor ranging from four to twenty and decreased as the vacuum improved. An intermittent vertical instability was also observed. The emittance increase and instability behavior depended strongly on beam current, pressure, number or bunches in the ring, duty cycle, store time and betatron tunes. This section is a summary of the observations made in a variety of conditions that are discussed in detail by Krejcik *et al* [30]and Zimmermann *et al*.[31]

A betatron tune shift indicating the trapping of ions was observed for a single, stored bunch when the population decayed below 1.5×10^{10} particles. This trapping threshold suggests an ion mass of about 40 – 50 AMU. The ion-induced tune shift of about 0.02, detected with two bunches, is consistent with an ion density equal to the residual gas density, confirming a postulate of Baconnier and Brianti that the gas density represents an upper limit on the accumulated ion density. [32]

By far the largest degradation of the beam quality occurred in the first few milliseconds after injection. A large emittance growth was observed in a parameter regime where ions could not be stably trapped. Figure DR8 shows that the emittance blow-up of the extracted beam, 8.3 msec after injection, was much larger for two bunches than for one and that there were large, non-Gaussian tails for two bunches. The extracted vertical beam size for two bunches and 8.3 msec store depended on the vertical betatron tune. These were consequences of a transverse instability that is a transient ion effect. The ions were trapped immediately after injection when the beam sizes were large, and later, as the beam size shrank and the ions become unstable, they caused a coherent instability. The non-Gaussian shape is expected as a result of filamentation in transverse phase space induced by a collective instability.[33]

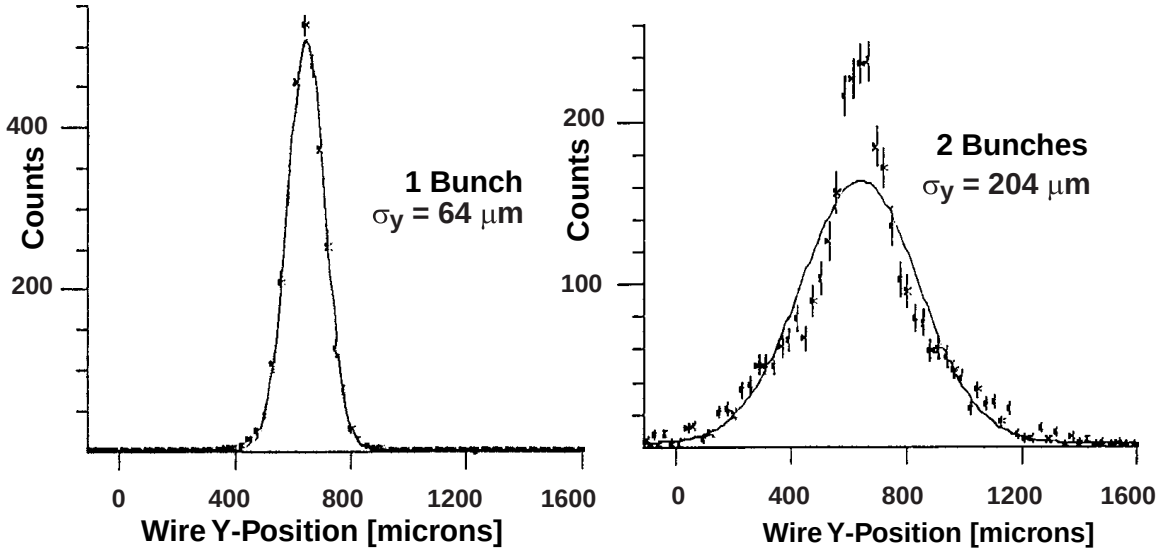

Figure DR8: Vertical beam sizes measured with a wire scanner in the extraction line for 8.3 msec store time.

Transverse beam-transfer function measurements with one and two bunches stored showed that the beam blow-up was a coupled bunch instability. The ion cloud would couple the transverse motion of the two bunches in either a 0- or a π-mode. The difference in frequencies of the two modes was a measure of the coupling strength.[30]

Although the vacuum never fully recovered after the catastrophic vent, it has recovered sufficiently that close to nominal emittances are achieved under certain operating conditions. With a long, 16.6 msec, store time the beam size damps sufficiently that ions are no longer stable and are completely expelled.* At the shorter 8.3 msec store time ions can be expelled with an appropriate choice of vertical betatron tune. When the vertical tune is set slightly below the half-integer, the higher π-mode frequency of the ion cloud coincides with the unstable ½-integer resonance. The ions are cleared, and the extracted beam emittance is close to nominal. This vertical tune is now routinely used.

Other ion related effects have been observed. Even when the beam was stored over extended periods of time, self-excited betatron sidebands were observed. These were taken as evidence of a residual persistent instability. The sidebands disappeared when the current decreased to about 10^{10} particles per bunch. However, the observed tune shifts, tune spreads and instability threshold could only partly be explained by the classical theory of a two-stream instability.[34,35,36]

All of these ion effects could be important in future fast-cycling rings, for example, in the damping rings of a next-generation linear collider.

---

* Comparison of vertical beam sizes with short and long stores has become a routine diagnostic of vacuum problems in the electron damping ring.

---

[1] G. Gross and J. Spencer in *4th European Particle Accelerator Conference,* 1994, edited by V. Suller and Ch. Petit-Jean-Genez, (World Scientific, , 1994), p. 2256.

[2] Roger Erickson, Editor, SLAC, SLC Design handbook (1984).

[3] R. L. Holtzapple, Stanford University, Longitudinal Dynamics at the Stanford Linear Collider (1996).

[4] T. Limberg, H. Moshammer, T. Raubenheimer, J. Spencer, R. Siemann in *3rd European Particle Accelerator Conf.,* 1992, edited by H. Henke, H. Homeyer, C. Petit-Jean-Genaz, (Editions Frontieres, , 1992), p. 682.

[5] P. Krejcik et al in *1993 Particle Accelerator Conference,* 1993, edited by S. T. Corneliussen, (IEEE, Piscataway, NJ, 1993), p. 3240.

[6] K. L. F. Bane ***et al*** in *1995 Particle Accelerator Conference,* 1995, edited by L. T. Gennari, (IEEE, Piscataway, NJ, 1996), p. 3105.

[7] K. L. F. Bane in *1st European Particle Accelerator Conference,* 1988, edited by S, Tazzari, (World Scientific, , 1989), p. 637.

[8] K. L. F. Bane and C. K. Ng in *1993 Particle Accelerator Conference,* 1993, edited by S. T. Corneliussen, (IEEE, Piscataway, NJ, 1993), p. 3432.

[9] B. V. Podobedov and R. H. Siemann, Phys. Rev. ST Accel. Beams **1**, 072801 (1998). (In print)

[10] F. J. Decker, C. E. Adolphsen, B. Podobedov, P. Raimondi in *18th International Linac Conference,* 1996, edited by C. Hill & M. Vretenar, (CERN, Geneva, Switzerland, 1996), p. 143.

[11] T. S. Mattison, R. L. Cassel, A. R. Donaldson and G. Gross in *1995 Particle Accelerator Conference,* 1995, edited by L. T. Gennari, (IEEE, Piscataway, NJ, 1996), p. 1915.

[12] J. Bijleveld et al, SLAC, SLAC-PUB-4028 (1986).

[13] M. A. Allen, H. D. Schwarz and P. B. Wilson, IEEE Trans. Nucl. Sci. **30**, 3447 (1983). (In print)

[14] F. Pedersen, IEEE Trans. Nucl. Sci. **22**, 1906 (1975). (In print)

[15] K. W. Robinson, Cambridge Electron Accelerator, CEAL-1010 (1964).

[16] P. Krejcik et al in *1993 Particle Accelerator Conference,* 1993, edited by S. T. Corneliussen, (IEEE, Piscataway, NJ, 1993), p. 2370.

[17] Y.-C. Chao et al in *1991 Particle Accelerator Conference,* 1991, edited by L. Lizama & J. Chew, (IEEE, Piscataway, NJ, 1991), p. 1806.

[18] R. E. Stege Jr., R. K. Jobe and M. Ross in *1993 Particle Accelerator Conference,* 1993, edited by S. T. Corneliussen, (IEEE, Piscataway, NJ, 1993), p. 2234.

[19] H. Schwarz and J. Judkins in *1987 Particle Accelerator Conference,* 1987, edited by E. R. Lindstrom and L. S. Taylor, (IEEE, Piscataway, NJ, 1987), p. 769.

[20] M. Minty ***et al*** in *1992 Accelerator Instrumentation Workshop,* 1992, edited by J. A. Hinkson and G. Stover, (AIP, Woodbury, NY, 1992), p. 158.

[21] M. Minty and R. Siemann, Nucl. Instr. and Meth. A **376**, 301 (1996). (In print)

[22] F. J. Decker, T. Limberg and J. L. Turner, Int. J. Mod. Phys. A **Proc. Suppl 2A**, 148 (1993). (In print)

[23] G. White, T. Himel, H. Shoaee in *1997 Particle Accelerator Conference,* 1997, edited by M. Comyn, M. K. Craddock, M. Reiser and J. Thomson, (IEEE, Piscataway, NJ, 1998), p. 2425.

[24] M. D. Woodley, L. Sanchez-Chopitea and H. Shoaee in *1987 Particle Accelerator Conference,* 1987, edited by E. R. Lindstrom and L. S. Taylor, (IEEE, Piscataway, NJ, 1987), p. 722.

[25] M. G. Minty and W. L. Spence in *1995 Particle Accelerator Conference,* 1995, edited by L. T. Gennari, (IEEE, Piscataway, NJ, 1996), p. 536.

[26] F. J. Decker ***et al*** in *3rd European Particle Accelerator Conf.,* 1992, edited by H. Henke, H. Homeyer, C. Petit-Jean-Genaz, (Editions Frontieres, , 1992), p. 342.

[27] C. Simopoulos and R. L. Holtzapple in *1995 Particle Accelerator Conference,* 1995, edited by L. T. Gennari, (IEEE, Piscataway, NJ, 1995), p. 3073.

[28] B. V. Podobedov and R. H. Siemann in *1997 Particle Accelerator Conference,* 1997, edited by M. Comyn, M. K. Craddock, M. Reiser and J. Thomson, (IEEE, Piscataway, NJ, 1998), p. 1629.

[29] E. Babenko, R. K. Jobe, D. McCormick, and J. T. Seeman in *1993 Particle Accelerator Conference,* 1993, edited by S. T. Corneliussen, (IEEE, Piscataway, NJ, 1993), p. 2423.

[30] P. Krejcik, D. Pritzkau, T. Raubenheimer, M. Ross and F. Zimmermann in *1997 Particle Accelerator Conference,* 1997, edited by M. Comyn, M. K. Craddock, M. Reiser and J. Thomson, (IEEE, Piscataway, NJ, 1998), p. 1626.

[31] F. Zimmermann et al in *International Workshop on Multi-Bunch Instabilities in Future Electron and Positron Accelerators,* 1997, edited by Y. H. Chin, (KEK, Tsukuba, Japan, 1997), p. 88.

[32] Y. Baconnier and G. Brianti, CERN, CERN/SPS/80-02 (DI) (1980).

[33] T. Raubenheimer, F.-J. Decker and J. Seeman in *1995 Particle Accelerator Conference,* 1995, edited by L. T. Gennari, (IEEE, Piscataway, NJ, 1995), p. 3291.

[34] G. Koshkarev and XXX. Zenkevich, Particle Accelerators **3**, 1 (1972). (In print)

[35] J. M. Laslett, A. M. Sessler and D. Mohl, Nucl. Instr. and Meth. **121**, 517 (1974). (In print)

[36] R. Alves Pires et al in *1989 Particle Accelerator Conference,* 1989, edited by XXX, (IEEE, Piscataway, NJ, 1989), p. 800.